Real-Time Observation of Formation and Relaxation Dynamics of NH_4 in $(CH_3OH)_m(NH_3)_n$ Clusters

Yuji Yamada, Yoko Nishino, Akimasa Fujihara, Haruki Ishikawa, and Kiyokazu Fuke*

Department of Chemistry, Graduate School of Science, Kobe University, Nada-ku, Kobe 657-8501, Japan

Received: November 22, 2008; Revised Manuscript Received: January 19, 2009

The formation and relaxation dynamics of $NH_4(CH_3OH)_m(NH_3)_n$ clusters produced by photolysis of ammonia−methanol mixed clusters has been observed by a time-resolved pump−probe method with femtosecond pulse lasers. From the detailed analysis of the time evolutions of the protonated cluster ions, $NH_4^+(CH_3OH)_m(NH_3)_n$, the kinetic model has been constructed, which consists of sequential three-step reaction: ultrafast hydrogen-atom transfer producing the radical pair $(NH_4-NH_2)^*$, the relaxation process of radical-pair clusters, and dissociation of the solvated NH_4 clusters. The initial hydrogen transfer hardly occurs between ammonia and methanol, implying the unfavorable formation of radical pair, $(CH_3OH_2-NH_2)^*$. The remarkable dependence of the time constants in each step on the number and composition of solvents has been explained by the following factors: hydrogen delocalization within the clusters, the internal conversion of the excited-state radical pair, and the stabilization of NH_4 by solvation. The dependence of the time profiles on the probe wavelength is attributed to the different ionization efficiency of the $NH_4(CH_3OH)_m(NH_3)_n$ clusters.

I. Introduction

The photoionization process of ammonia clusters has been an attractive issue for a long time and has been extensively investigated by means of numerous experimental techniques such as electron impact [1−3] and photon ionization.[4−8] The mass spectra obtained after ionization of $(NH_3)_n$ clusters show the predominance of the protonated clusters, $NH_4^+(NH_3)_n$. Except for a single-photon ionization, in which the photon energy is close to the threshold,[9] unprotonated $(NH_3)_n^+$ cluster ions are observed very weakly. Various experimental [10−15] and theoretical studies [16−21] have suggested the formation of the $NH_4^+(NH_3)_n$ ion signal through two processes (Scheme 1) in the resonant two-photon ionization of $(NH_3)_n$. The first process is the significantly fast process including proton transfer and fragmentation from $(NH_3)_n^+$ with higher internal energy (process A). The second is the production of $NH_4^+(NH_3)_n$ through the ionization of the long-lived $NH_4(NH_3)_n$ radical clusters which are formed by hydrogen-atom transfer (H-T) and NH_2 fragmentation within $(NH_3)_n$ excited to the first electronically excited state (Ã-state) (process B). This excited-state dynamics includes the ultrafast predissociation of the Ã-state ammonia, $NH_3 \rightarrow NH_2 + H$, with a lifetime of less than 200 fs.[22,23] In 1993, Castleman and co-workers investigated the photoionization of $(NH_3)_n$ by means of a time-resolved pump−probe method and revealed that the Ã-state ammonia clusters predissociate rapidly and produce the long-lived $NH_4(NH_3)_n$ clusters.[24,25] Fuke and Takasu have observed that the time evolution of unprotonated dimer ion signal $(NH_3)_2^+$ exhibits a rise feature corresponding to the formation of $(NH_4-NH_2)^*$, i.e., the evidence of H-T.[26] Hertel and co-workers have also measured the time evolutions of various ion signals and explained the results by constructing a sophisticated kinetic model.[27] These experimental studies have suggested that $NH_4(NH_3)_n$ radical clusters are formed by process B in Scheme 1.

SCHEME 1

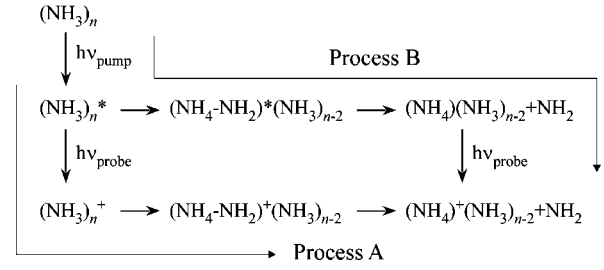

Concerning the long-lived solvated NH_4 radical clusters, NH_4 has been known to be a typical Rydberg radical having one 3s electron [28−30] and is isoelectronic with Na atom. Thus, similarly to the extensive studies on the solvated Na clusters,[31−34] the solvation effect of the NH_4 radical clusters is an attractive issue related to the subject of microscopic solvation process. In our previous works, we have investigated the structure and stability of the NH_4 radical solvated by ammonia and water using an ionization potential (IP) and electronic spectra measurements.[35−37] From the comparison with the theoretical works by Kassab et al.[38,39] and Daigoku et al.,[40] it has been concluded that the larger $NH_4(NH_3)_n$ clusters form a one-center Rydberg-like ion pair, where the NH_4^+ core is surrounded by NH_3 solvents and the 3s electron is delocalized at the cluster surface. On the other hand, the recent IP measurements and *ab initio* calculations on $NH_4(CH_3OH)_m(NH_3)_n$ have revealed that methanol is likely to form a hydrogen-bond network, and as a result, the one-center ion-pair formation is unfavorable in these clusters.[41] Although the structures of these clusters have been studied extensively, the generation and relaxation mechanisms of $NH_4(CH_3OH)_m(NH_3)_n$ clusters still remain to be unveiled. Especially, it is worth examining the lifetimes of $NH_4(CH_3OH)_m$ in order to understand the relaxation dynamics including a hydrogen-atom migration within clusters.

In the present work, we have investigated the formation and decay processes of $NH_4(CH_3OH)_m(NH_3)_n$ ($m \leq 3$, $n \leq 4$) after photolysis of the jet-cooled ammonia−methanol mixed clusters

* To whom orrespondence should be addressed. E-mail: fuke@kobe-u.ac.jp.

10.1021/jp810266a CCC: $40.75
Published on Web 02/26/2009

in a supersonic jet using time-resolved pump−probe spectroscopy with femtosecond laser. The observed time evolutions of the $NH_4^+(CH_3OH)_m(NH_3)_n$ ion signals have been analyzed by a kinetic model composed of three decay components: the predissociation of the $\tilde{A}$-state ammonia molecule, the relaxation of radical pair $(NH_4-NH_2)^*$ including the NH_2 dissociation, solvent evaporation, and internal conversion, and the dissociation of NH_4 radical clusters via hydrogen-atom tunneling reaction. In addition, it has been found that the unprotonated ammonia dimer ion, $(NH_3)_2^+$, exhibited a rise curve component, which is clear evidence of the formation of a radical pair. On the other hand, we have observed no $(CH_3OH-NH_3)^+$ signal, which implies that the H-T between ammonia and methanol molecules to produce a radical pair, $CH_3OH_2-NH_2$, does not occur. We have examined the dependence of the time constants in each step on the number or composition of solvents. On the basis of these results, we have discussed the formation and relaxation dynamics of $NH_4(CH_3OH)_m(NH_3)_n$.

II. Experimental Section

A detailed description of the experimental setup is given in the previous paper.[26] In brief, the system consists of a three-stage differentially evacuated chamber which includes a cluster source and a reflectron-type time-of-flight (TOF) mass spectrometer. The ammonia−methanol mixed clusters were generated by a supersonic expansion of methanol vapor at room temperature seeded in pure ammonia carrier gas (typically 2 atm) into vacuum through a pulsed nozzle (General valve, series 9) having a 0.8 mm aperture. The free jet was skimmed by a skimmer located at 30 mm downstream of the nozzle. Neutral clusters were introduced into the acceleration and photoionization regions of the reflectron TOF mass spectrometer.

In the time-resolved pump−probe experiments, femtosecond laser pulses were generated by a diode laser pumped Ti:Sapphire laser (Spectra Physics, TSUNAMI). The output was amplified by a commercial regenerative amplifier (Spectra Physics, Spitfire) pumped by a 10 Hz Nd:YAG laser (Quantum-Ray, GCR-150). The wavelength was tuned to 790 nm. At this wavelength, a pulse duration was typically 120 fs fwhm and a pulse energy was about 6 mJ/pulse. The pump pulse at 197 nm was generated by a phase-matched sequential conversion of the 790 nm pulse with three BBO crystals arranged in a nonlinear sum-frequency mixing scheme. The energy of the pump pulse was typically 2 μJ/pulse. The pulse duration was obtained to be 400 fs (fwhm) from a cross-correlation measurement with the third harmonic pulse at 263 nm. The second and third harmonic pulses at 395 and 263 nm, respectively, were used as the probe pulses, which were attenuated to 20−50 μJ/pulse to avoid a multiphoton ionization process. The pump and probe pulses were separated by a 45° reflecting mirror, and the latter was delayed by a computer-controlled optical delay line. Thereafter, both pulses were recombined by using another 45° high reflector. The laser beams were introduced into the interaction region in the vacuum chamber without focusing, and ionized the clusters in a supersonic beam at 150 mm downstream of the skimmer. The photoionized cluster ions were accelerated and collimated by ion optics and were detected by dual microchannel plates (HAMAMATSU Photonics, F1552-23S). The output signals were fed into a digital storage oscilloscope (LeCroy 9310C) after a wide-band amplifier (NF Electronic Instruments, BX-31). The mass spectra were measured at various delay times between the pump and probe pulses.

The methanol (99.0%) was purchased from Wako Chemicals Industry Ltd. and was used without purification. The ammonia (>99.99%) was purchased from Nippon Sanso.

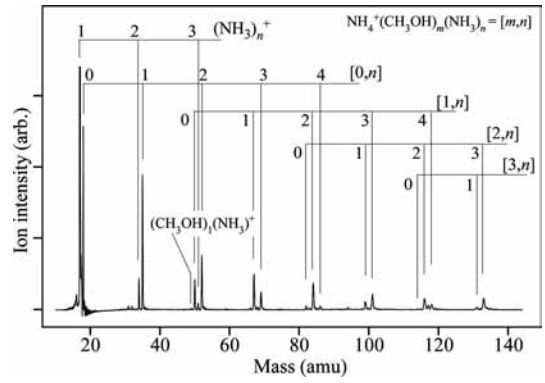

Figure 1. Typical TOF mass spectrum obtained by irradiation of the probe laser pulse (263 nm) at the delay time of 100 fs after photolysis of methanol−ammonia mixed cluster by pump pulses (197 nm).

III. Results

A. Mass Spectrum. A typical TOF mass spectrum obtained by irradiation of the probe pulse at the delay time of 100 fs after the photolysis of methanol−ammonia mixed clusters by the pump pulse is shown in Figure 1. It consists of a series of $NH_4(CH_3OH)_m(NH_3)_n^+$ ($m \leq 3$, $n \leq 4$) ions, unprotonated $(NH_3)_n^+$ ($n \leq 3$) ions, and a very weak $(CH_3OH)_1(NH_3)_1^+$ ion signal. Since the durations of the pump pulses in this experimental setup are about 400 fs, two laser pulses are temporally overlapped at this delay time. The overlapped pulses excite the NH_3 moiety in the neutral clusters to the excited state and simultaneously ionize the $\tilde{A}$-state NH_3, leading to strong intensity of NH_3^+ ion. However, CH_3OH^+ is not observed, implying that the resonant two-photon ionization via the excited electronic state of methanol does not occur. This is because the wavelength of the pump pulse is far from the $\tilde{A}-\tilde{X}$ transition of methanol at 161 nm.[42] Thus, it is considered that the H-T process in the clusters occurs on the excited state of ammonia as follows

$$(CH_3OH)_m(NH_3)_{n+1} + h\nu_{pump} \rightarrow (CH_3OH)_m(NH_3)_n-NH_3^* \rightarrow [H(CH_3OH)_m(NH_3)_n-NH_2]^* \quad (1)$$

B. Time Profiles for $NH_4(CH_3OH)_m(NH_3)_n$. Figure 2 shows the time evolutions of $NH_4^+(CH_3OH)_m(NH_3)_n$ (m, $n \leq 1$) and $(CH_3OH)_m(NH_3)_n^+$ ($m \leq 1$, $n \leq 2$) after the excitation to the first excited state. The time profiles in the left column are measured with the fine scan over 4.5 ps with a step of 50 fs in order to clearly display the sharp spike for NH_3^+, corresponding to the ultrafast decay of the $\tilde{A}$-state NH_3 (<200 fs). The time profile is almost symmetric and close to a cross-correlation curve of two laser pulses. In contrast to NH_3^+, NH_4^+ has a slower decay component in addition to the sharp spike. The middle and right columns in Figure 2 show the time profiles with a step of 250 fs. Similarly to NH_4^+, $NH_4^+(NH_3)_n$ and $NH_4^+(CH_3OH)_m$ exhibit the slower decay component, while the time profiles of unprotonated species are different from them. $(NH_3)_2^+$ exhibits a rise feature in addition to the sharp spike, which is the same as the results in the previous experiments for the pure ammonia system,[26,27] while the rise feature is not observed for $(CH_3OH)(NH_3)^+$. This finding will be an important key to interpret the dependence of dynamics on the solvation.

We also investigate the dependence of time evolution on the number and composition of solvents. The time evolutions of $NH_4^+(CH_3OH)_m(NH_3)_n$ ($m \leq 2$, $n \leq 3$) on a longer time scale with a step of 0.53 ps are shown in Figure 3. The sharp spike

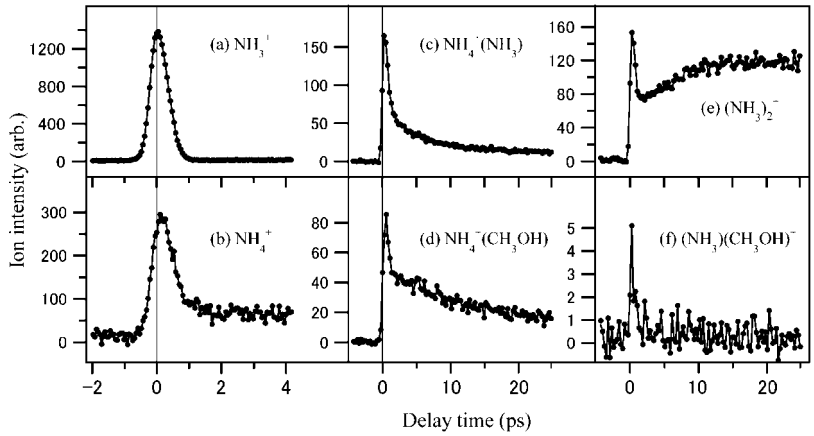

Figure 2. Time evolutions of (a) NH_3^+, (b) NH_4^+, (c) $NH_4^+(NH_3)$, (d) $NH_4^+(CH_3OH)$, (e) $(NH_3)_2^+$, and (f) $(NH_3)(CH_3OH)^+$ ion signals.

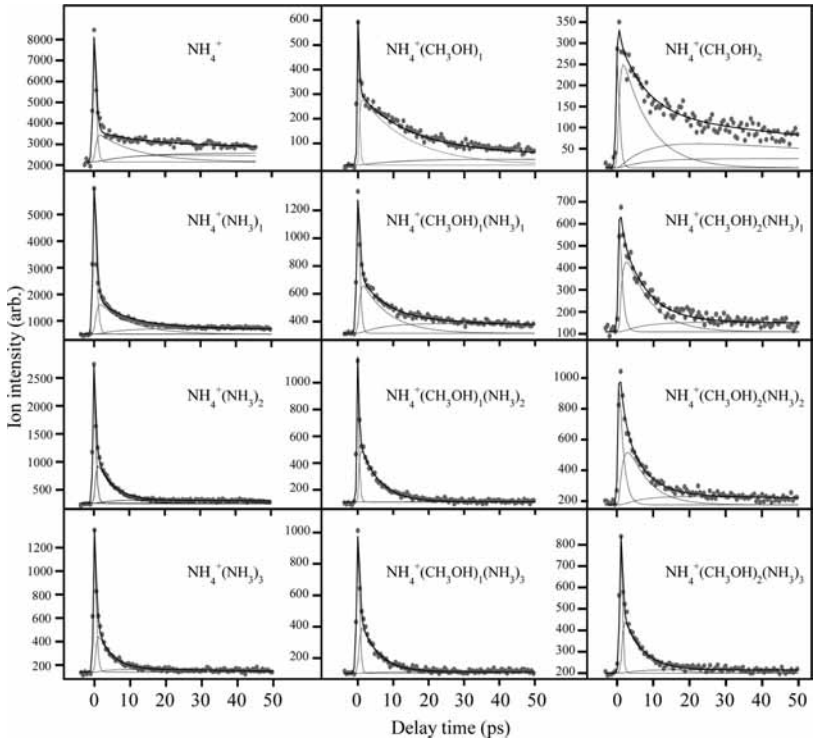

Figure 3. Time evolutions of $NH_4^+(CH_3OH)_m(NH_3)_n$ ion signals. The solid curves are the convoluted ones by means of the constructed kinetic model and the time constants listed in Table 2.

and the slower decay component are observed for these clusters. The latter component does not completely reach zero at longer delay time. The amplitudes of these long tails depend on the number of solvents; they decrease with increasing ammonia molecules. Note that the amplitude ratios of the former to the latter decrease with the addition of methanol molecules. These features of the time evolution for the slower decay components may be important to understand the generation and relaxation dynamics of $NH_4(CH_3OH)_m(NH_3)_n$ clusters.

In the case of the unprotonated dimer, $(NH_3)_2^+$, as seen in Figure 4, the slow-decay component is also observed on the longer scale over 30 ps in addition to the rise feature in Figure 2e. On the other hand, the pump−probe curves of trimers, $(NH_3)_3^+$ and $(CH_3OH)_1(NH_3)_2^+$, resemble those of $NH_4^+(CH_3OH)_m(NH_3)_n$, which consist of the sharp spike and the slower decay components. The similarity in the time profiles of these clusters seems to imply that the protonated and unprotonated ions are formed by ionization of the same radicals produced through the common dynamics, which will be explained in detail by construction of the kinetic model.

C. Time Profiles on a Longer Time Scale. We are also interested in the slower dynamics, i.e., the time evolution of the slowly decaying long tail observed in Figure 3. This dynamics corresponds to the relaxation of $NH_4(CH_3OH)_m(NH_3)_n$ radicals, which is predicted to be on the order of picosecond to microsecond. Figure 5 shows the pump−probe curves of $NH_4^+(CH_3OH)_m(NH_3)_n$ ($m \leq 2$, $n \leq 2$) and $(NH_3)_2^+$ as a function of the delay time up to 500 ps with a step of 6.6 ps. Here, we focus on the curves after 100 ps, where only the decomposition process of the solvated NH_4 radical cluster is responsible for the observed dynamics, as discussed previously by Fuke and Takasu.[26] We have fitted the curve after 100 ps to a superposition of a single-exponential decay and a step function and have obtained the time constants summarized in Table 1. As shown by the solid curves in the figure, the fittings reproduce the experimental data well. The time profiles of NH_4^+ and its solvated cluster ions with methanol molecules have the short lifetimes of about 300 ps, while the solvation of more than one ammonia molecule elongates the lifetimes to longer than 10 ns, which is the longest lifetime determined accurately on this

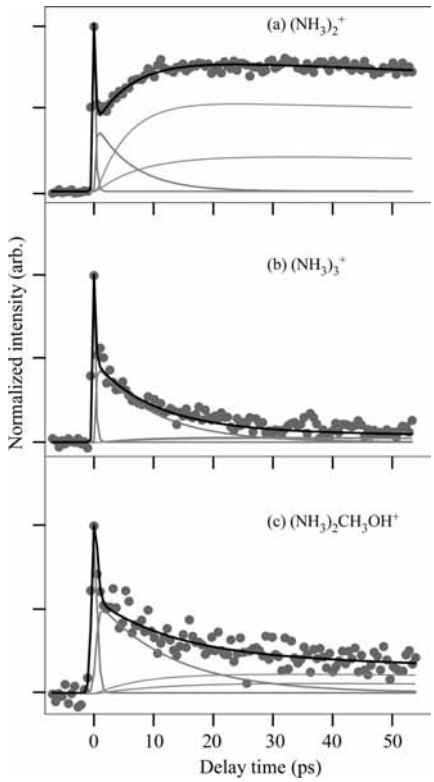

Figure 4. Time profiles of the unprotonated ions, (a) $(NH_3)_2^+$, (b) $(NH_3)_3^+$, and (c) $(NH_3)_2CH_3OH^+$. The thick solid curves are the ones calculated by means of the time constants listed in Table 2. The gray curves correspond to the time evolution of each state.

TABLE 1: Time Constants (ns) Obtained from Time Profiles with the Longer Delay Scan of $NH_4(CH_3OH)_m(NH_3)_n^+$ and $(NH_3)_2^+$ Ion Signals Assuming a Single-Exponential Decay

	$NH_4^+(CH_3OH)_m(NH_3)_n$			
n	$m = 0$	$m = 1$	$m = 2$	$(NH_3)_2^+$
0	0.23 ± 0.02	0.30 ± 0.04	0.35 ± 0.05	0.34 ± 0.03
1	>10	>10	>10	
2		>10	>10	

scan scale. The extensive elongation of lifetime of NH_4 by the addition of ammonia agrees with the previous results that the lifetime of NH_4 radical is elongated from 13 ps to 3 μs by the solvation of one NH_3.[26] This result also implies the very long lifetimes of the large size clusters with ammonia, as predicted by Bobbert et al. from the detection of the large ammonia clusters by resonant two-photon ionization process with nanosecond laser pulses.[43]

D. Dependence of Time Profiles on the Probe Wavelength. Figure 6 shows the time evolutions of $NH_4^+(CH_3OH)_m(NH_3)_n$ with the probe wavelength at 395 nm. For comparison, the temporal evolutions of $NH_4^+(CH_3OH)_1(NH_3)_n$ ($n = 0-4$) with the 263 nm probe are also plotted in this figure as red open circles. As seen in the figure, the intensity of the long tail for $NH_4(CH_3OH)_1(NH_3)_1^+$ is close to zero in the case of 395 nm, while the curve probed at 263 nm exhibits the significant intensity. The difference in the time profiles with two probe wavelengths becomes smaller with increasing the number of ammonia, and finally, they become coincident for $NH_4^+(CH_3OH)_1(NH_3)_n$ ($n = 3, 4$).

Since the IPs of $NH_4(CH_3OH)_m(NH_3)_n$ ($m, n \leq 1$) are 4.6−3.6 eV,[41] these clusters cannot be ionized by one-photon process with the 395 nm probe laser. The radical pair and its clusters also have fairly high IP, [26] and it is difficult to ionize these species by one photon of the 395 nm probe pulse. In order to gain signal intensities for the long-lived components, the time profiles for $NH_4^+(CH_3OH)_m(NH_3)_n$ ($m + n \leq 1$) ions are measured by focusing the probe laser with a lens of 500 mm focal length. Therefore, the ion signals of these clusters are mainly generated by two-photon process. The similar pump−probe study of $NH_4(NH_3)_n$ has also been reported by Freudenberg et al.[44] They have found the significantly different time profile for NH_4^+ compared with those for the larger clusters with using the 400 nm probe wavelength. They have suggested that the different decay of NH_4^+ might arise from the ion signal by the absorption of two probe photons from some low-lying excited levels. Thus, in order to avoid the complication of constructing a kinetic model, we confine the probe process to one-photon absorption without a lens.

IV. Discussion and Analysis

A. Initial Dynamics: Hydrogen-Atom Transfer. Before discussing the kinetic model, we focus on the initial dynamics after the excitation by the pump photons. The sharp spike of NH_3^+ and the rise feature of $(NH_3)_2^+$ in Figure 2 are coincident with the previous works.[26,27] The former corresponds to the ultrafast decay of the $\tilde{A}$-state of the NH_3 moiety excited initially by pump pulse and is consistent with the predissociation rate of the $\tilde{A}$-state ($\nu'_2 = 5$) of ammonia (<100 fs).[22] On the other hand, the latter corresponds to the generation of an excited-state radical pair, $(NH_4-NH_2)^*$, which is formed through the dissociation of the $\tilde{A}$-state ammonia followed by the ultrafast H-T between NH_3-NH_3. As seen in Figure 2e, however, the rise component is not observed in the time profile for $NH_3(CH_3OH)^+$. This result implies that the radical pair of $CH_3OH_2-NH_2$ is not formed and that H-T between CH_3OH and NH_3 is unfavorable.

In both cases of NH_3-NH_3 and CH_3OH-NH_3, the dissociation of hydrogen atom from the excited NH_3^* occurs, but the difference in a hydrogen-atom affinity between NH_3 and CH_3OH gives different reaction behavior. This difference may be intimately related to that in the stability between NH_4 and CH_3OH_2. Concerning to this issue, Williams and Porter reported the stabilization of the RH_2 radicals ($RH_2 = CH_5$, H_3O, and NH_4) produced by electron capture interaction of RH_2^+ ion with Na or K atoms.[45−47] They have predicted the dissociative lifetimes of these radicals to be less than 10^{-7} s, suggesting that these radicals might be unstable with respect to the hydrogen-atom dissociation. Moreover, Chen and Davidson calculated the potential curves of NH_4 and H_3O along the R−H bond cleavage. The calculated barrier heights were reported to be 0.267 and 0.004 eV for NH_4 and H_3O, respectively.[48] Although a barrier height of CH_3OH_2 is not available, it is reasonable to consider that CH_3OH_2 is unstable as in the case of H_3O.

It is interesting to note that the sharp spike is also observed in the time profile for $NH_3(CH_3OH)^+$ ion, though the initial dynamics of CH_3OH-NH_3 includes no H-T reaction. The observed spike may be attributed to the dissociation of hydrogen atom as follows

$$CH_3OH-NH_3 + h\nu_{pump} \rightarrow CH_3OH-NH_3^* \rightarrow CH_3OH + NH_2 + H \quad (2)$$

Therefore, the sharp spike in the time profile for $(CH_3OH)(NH_3)^+$ indicates that the hydrogen-atom elimination

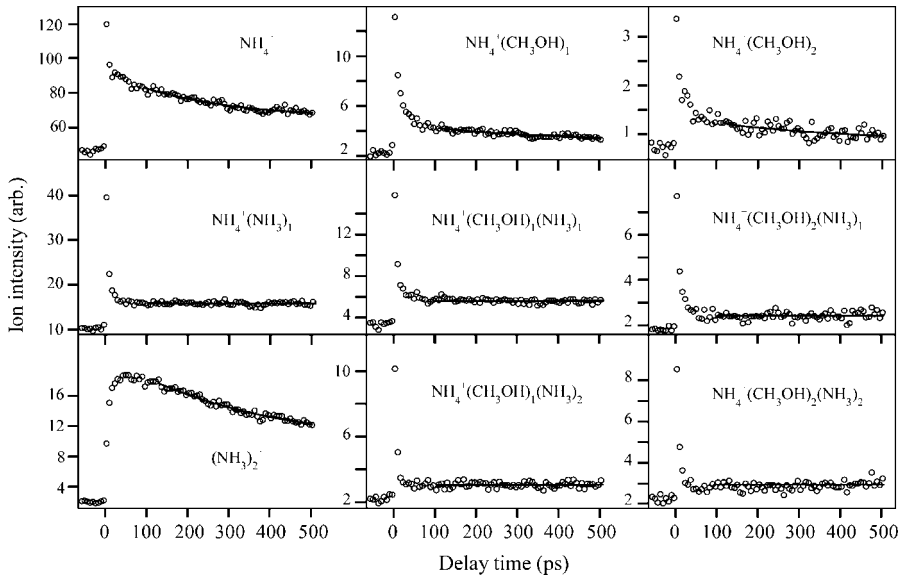

Figure 5. Time evolutions of $NH_4^+(CH_3OH)_m(NH_3)_n$ and $(NH_3)_2^+$ ion signals on a longer time scale. The solid curves display the fitting results by assuming the single-exponential decay function.

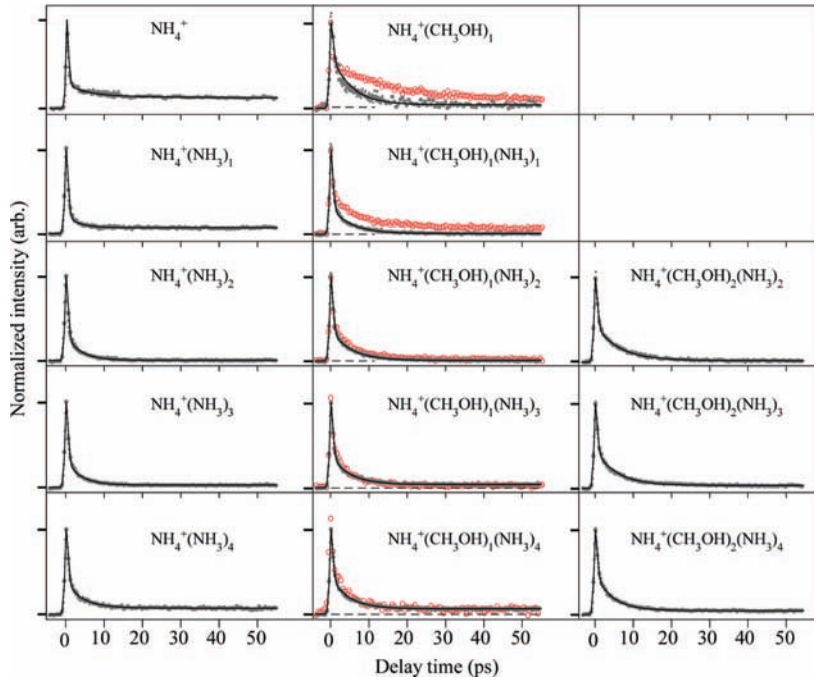

Figure 6. Time profiles of $NH_4^+(CH_3OH)_m(NH_3)_n$ ion signals with the longer probe wavelength (395 nm). The solid curves are the ones simulated by using the time constants listed in Table 3. For comparison, the time profiles measured with a shorter probe wavelength (263 nm) are shown by red open circles.

is also very fast in the CH_3OH-NH_3 system and completes within <300 fs.

B. Preparation of the Kinetic Model. In order to examine the contribution of solvent number and composition to the time evolution of each ion signal, the time constants for the generation and relaxation steps of NH_4 are derived by constructing an appropriate kinetic model. Since the observed time evolutions include not only the excited-state dynamics of neutral clusters but also the fragmentation after the ionization from neutral states, the analyses of time profiles are considered to be complicated. However, Hertel and co-workers have made an effort to construct a sophisticated model for the generation and relaxation processes of $NH_4(NH_3)_n$.[27] Their model has reproduced the rise feature of $(NH_3)_2^+$ and the decay curves of $NH_4^+(NH_3)_n$ ion signals very well, which are also observed in the present experiments. Thus, their kinetic model may also be very useful to discuss the time profiles of our mixed-solvent system. In the following paragraph, the construction of the kinetic model is described in detail.

Figure 7shows the sequential kinetic scheme and energy diagram considered in the fitting of the experimental data. After the initial excitation from the ground state to the Ã-state of NH_3 (state **1**), a fast H-T from the excited NH_3* to the neighboring NH_3 to form (NH_4NH_2)* (state **2**) occurs with a rate of k_{12}. As stated above, the fragmentation to a loss channel (X) competes with H-T. In the loss channel, most

of the excess energy in the generated clusters is removed by dissociation, and as a result, the probe photons no longer ionize the produced clusters. Following the H-T, three reactions are predicted to take place: an ejection of an NH_2 unit leading to the formation of the neutral ammonium radical clusters, $NH_4(CH_3OH)_m(NH_3)_n$ (state **3**), an evaporation of ammonia or methanol molecules to generate the relatively cooled radical pair (state **4**), and the other relaxation process to loss channel, such as internal conversion. Here, one may wonder whether the NH_4 radical is in the ground or excited state. The *ab initio* calculations by Park and Iwata for the electronic states of $(NH_3)_2$ have indicated that the excitation by 197 nm (6.28 eV) photons creates the first excited state of radical pair ($[NH_2-NH_4]$*; $^1A'$), correlating with an asymptote ($NH_4 + NH_2$*; $\tilde{A}^2A_1$).[19] In addition, total excitation energy is smaller by about 0.5 eV to produce the electronically excited state of NH_4 ($NH_2 + NH_4$*; $^2T_2$). Therefore, the generated NH_4 radical clusters are considered to be in the electronic ground state. In the final step, the NH_4 radical clusters and the cooled radical pairs relax to the loss channels (X and X′) by the hydrogen-atom elimination from NH_4 radical through a tunneling reaction process. The direct fragmentation of an NH_2 unit from the initial excited state, **1** → **3**, is also a possible candidate to explain the observed dynamics. Although this path cannot be excluded completely, it seems to be negligible compared to the paths, **1** → **2**, shown in Figure 7, because this direct path can be considered to be the same sequential reaction (**1** → **2** → **3**), in which the system paths through a higher-energy trajectory.

Based on the excitation scheme illustrated in Figure 7, we have constructed the rate equations for the time evolutions of the populations in the state **1** through **4**, $[S_1(t)]$ to $[S_4(t)]$, respectively, as follows

$$\frac{d[S_1(t)]}{dt} = -k_{12}[S_1(t)] - k_{10}[S_1(t)] = -(k_{12} + k_{10})[S_1(t)] \quad (3)$$

$$\frac{d[S_2(t)]}{dt} = k_{12}[S_1(t)] - k_{23}[S_2(t)] - k_{24}[S_2(t)] - k_{20}[S_2(t)] = k_{12}[S_1(t)] - (k_{23} + k_{24} + k_{20})[S_2(t)] \quad (4)$$

$$\frac{d[S_3(t)]}{dt} = k_{23}[S_2(t)] - k_{30}[S_3(t)] \quad (5)$$

$$\frac{d[S_4(t)]}{dt} = k_{24}[S_2(t)] - k_{40}[S_4(t)] \quad (6)$$

Here, it is easy to solve these rate equations by setting $k_{12} + k_{10} = K_1$, $k_{23} + k_{24} + k_{20} = K_2$, $k_{12} = c_1K_1$, $k_{23} = c_2K_2$, $k_{24} = c_2'K_2$, and $k_{20} = (1 - c_2 - c_2')K_2$. The above equations are rewritten, as follows

$$\frac{d[S_1(t)]}{dt} = -K_1[S_1(t)] \quad (7)$$

$$\frac{d[S_2'(t)]}{dt} = K_1[S_1(t)] - K_2[S_2'(t)] \quad (8)$$

$$\frac{d[S_3'(t)]}{dt} = K_2[S_2'(t)] - k_{30}[S_3'(t)] \quad (9)$$

$$\frac{d[S_4'(t)]}{dt} = K_2[S_2'(t)] - k_{40}[S_4'(t)] \quad (10)$$

where $[S_2'(t)] = [S_2(t)]/c_1$, $[S_3'(t)] = [S_3(t)]/c_1c_2$, and $[S_4'(t)] = [S_4(t)]/c_1c_2'$, respectively. From eqs 7−10, the time evolutions of the populations in the state **1** through **4** are easily calculated.

$$[S_1(t)] = W^{mn}\exp(-K_1t) \quad (11)$$

$$[S_2(t)] = c_1W^{mn}\frac{K_1}{K_1 - K_2}\{\exp(-K_2t) - \exp(-K_1t)\} \quad (12)$$

$$[S_3(t)] = \frac{c_1c_2W^{mn}K_1K_2}{(K_1 - K_2)(K_2 - k_{30})(K_1 - k_{30})} \times \{(K_1 - K_2)e^{-k_{30}t} - (K_1 - k_{30})e^{-K_2t} + (K_2 - k_{30})e^{-K_1t}\} \quad (13)$$

$$[S_4(t)] = \frac{c_1c_2'W^{mn}K_1K_2}{(K_1 - K_2)(K_2 - k_{40})(K_1 - k_{40})} \times \{(K_1 - K_2)e^{-k_{40}t} - (K_1 - k_{40})e^{-K_2t} + (K_2 - k_{40})e^{-K_1t}\} \quad (14)$$

where W^{mn} is the population of $(CH_3OH)_m(NH_3)_n$* in the initial Ã-state. The typical time evolutions of the populations are shown in Figure 8, where the curves are convoluted with the pulse width of 400 fs. In the calculations, we adopt appropriate parameters, such as $K_1 = (200\ fs)^{-1}$, $K_2 = (4\ ps)^{-1}$, $k_{30} = (10\ ns)^{-1}$, $k_{40} = (200\ ps)^{-1}$, $c_1 = 0.5$, $c_2 = 0.5$, and $c_2' = 0.5$. It is clear that the population change of the state **1** provides the sharp spike.

In addition to the dynamics among the neutral state **1** through **4**, a branching ratio of the fragmentation in ionic states should be taken into account. As have been shown by several groups,[4−8] the $(CH_3OH)_m(NH_3)_n^+$ ions generated via the excited state **1** forms the protonated ammonium cluster ions, $NH_4^+(CH_3OH)_m(NH_3)_{n-1} + NH_2$. Since the sharp spikes are observed in the time profiles for unprotonated ions, i.e., NH_3^+, $(NH_3)_2^+$, and $NH_3(CH_3OH)^+$, the formation of protonated ammonia cluster ions is not the sole product for the fragmentation of $(CH_3OH)_m(NH_3)_n^+$, but the process to form unprotonated ions proceeds competitively with small probability. The ionization of the radical-pair state **2** mainly produces the protonated ions accompanied by the fragmentation of NH_2 due to a large excess energy, which is consistent with the previous result that the unprotonated $(NH_3)_n^+$ ions are efficiently produced by ionization of the radical pair at 400 nm compared with that at 266 nm.[44] The branching and detection probabilities, p_{ip}^{mn} and p_{iu}^{mn} for the protonated and unprotonated ions generated after ionization from the state i of $(CH_3OH)_m(NH_3)_n$, respectively, are introduced to the fitting procedure. For example, p_{2p}^{mn} includes the ionization

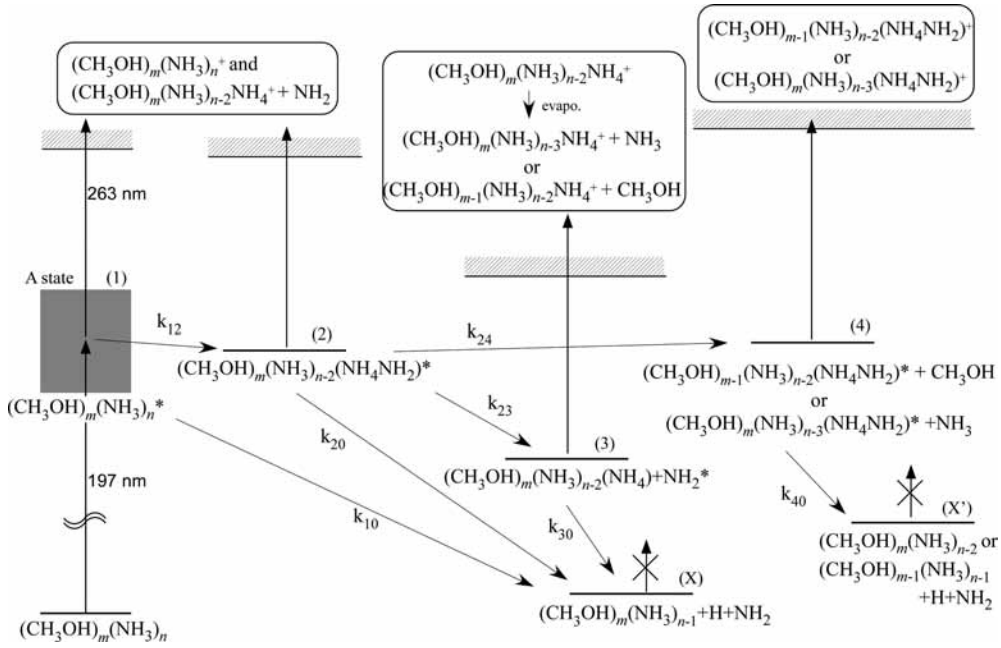

Figure 7. Kinetic model and energy diagram for the relaxation dynamics of the mixed ammonia−methanol clusters, $(CH_3OH)_m(NH_3)_n$, following the excitation. k_{ij} indicates the relaxation dynamics from the state i to j. The fragmentation dynamics in ionic state is also depicted. See text.

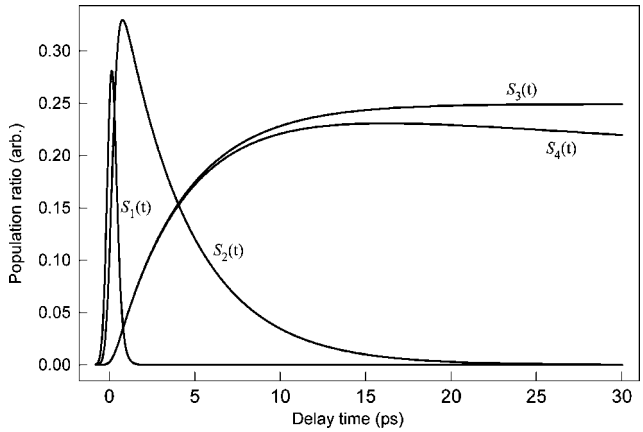

Figure 8. Typical example of the calculated time evolutions of population in the states **1** through **4** in the kinetic model described in Figure 7. $S_i(t)$ in the figure means the time evolutions of populations in the state i, represented by eqs 11−14. In this calculation, the parameters were assumed to be $W^{mn} = 1$, $K_1 = (200\ \text{fs})^{-1}$, $K_2 = (4\ \text{ps})^{-1}$, $k_{30} = (10\ \text{ns})^{-1}$, $k_{40} = (200\ \text{ps})^{-1}$, $c_1 = 0.5$, $c_2 = 0.5$, and $c_2' = 0.5$.

efficiency and branching ratio to produce the $NH_4^+(CH_3OH)_m(NH_3)_{n-2}$ after ionization of the state **2**, $(CH_3OH)_m(NH_3)_{n-2}(NH_4NH_2)^*$, generated by H-T of $(CH_3OH)_m(NH_3)_n^*$. On the other hand, p_{4p}^{mn} formally denotes the detection and branching ratio for $NH_4^+(CH_3OH)_m(NH_3)_n$ ionized from the state **4** of $(CH_3OH)_m(NH_3)_n(NH_4NH_2)^*$, which is an exceptional notation against the above definition. This is because the state **4** originating from the neutral $(CH_3OH)_m(NH_3)_n$ cluster includes two states of $(CH_3OH)_{m-1}(NH_3)_{n-2}(NH_4NH_2)^*$ and $(CH_3OH)_m(NH_3)_{n-3}(NH_4NH_2)^*$, so that it is invalid to apply the identical parameter p_{4p}^{mn} to two different radical pairs as in the original definition.

In addition to the above branching and detection probabilities, other branching probabilities should be introduced. In the ionic state after the ionization from the state **3**, the evaporation of solvent occurs, which may dissociate the terminal hydrogen bond resulting in fragmentation of a terminal solvent, which is an ammonia or a methanol. This branching ratio of the evaporation of an ammonia from $NH_4^+(CH_3OH)_m(NH_3)_n$ is given as a parameter b_a^{mn}. According to our previous study on the solvation structure of $NH_4(CH_3OH)_m(NH_3)_n$, a terminal ammonia is more favorable as an acceptor of hydrogen atom than a terminal methanol.[41] Therefore, it is reasonable to consider that the evaporation of an ammonia molecule occurs dominantly after ionization, although we cannot estimate the branching ratio of evaporation accurately. The solvent evaporation is also the central issue in the reaction step from the state **2** to **4** in the neutral state as well as the ionic state. The parameter d_a^{mn} corresponds to the branching ratio of an ammonia dissociation from the state **2** $(CH_3OH)_m(NH_3)_{n-2}(NH_4NH_2)^*$ cluster. Obvi-

TABLE 2: Lifetimes of the Initial Excited State of $(CH_3OH)_m(NH_3)_n^*$, the $(CH_3OH)_m(NH_3)_{n-2}(NH_4NH_2)^*$ Radical Pair, and the Subsequently Formed $NH_4(CH_3OH)_m(NH_3)_{n-2}$, Described by T_1 (fs), T_2 (ps), and τ_{30} (ps), Respectively[a]

	$T_1/T_2/\tau_{30}$		
n	$m = 0$	$m = 1$	$m = 2$
2	190^{+90}_{-50} / 8.1 ± 0.5 / 13[b]	300^{+70}_{-70} / 14.9 ± 0.6 / 230 ± 20	300^{+60}_{-70} / 9.6 ± 0.6 / 300 ± 40
3	200^{+90}_{-50} / 6.5 ± 0.3 / ≫10^4[c]	250^{+80}_{-60} / 8.3 ± 0.3 / ≫10^4[c]	350^{+50}_{-80} / 6.0 ± 0.5 / ≫10^4[c]
4	250^{+80}_{-60} / 4.0 ± 0.3 / ≫10^4[c]	290^{+70}_{-60} / 5.4 ± 0.3 / ≫10^4[c]	310^{+60}_{-60} / 4.2 ± 0.3 / ≫10^4[c]
5	270^{+70}_{-70} / 3.5 ± 0.2 / ≫10^4[c]	300^{+60}_{-70} / 4.2 ± 0.3 / ≫10^4[c]	340^{+50}_{-70} / 3.0 ± 0.3 / ≫10^4[c]

[a] Time constants are derived by least-squares fittings of the time profiles with the probe of 263 nm. [b] Fuke et al., ref 26. [c] These values cannot be determined accurately because of their very long lifetimes. See text.

ously, in the case of the clusters containing no ammonia molecule ($n = 2$), only methanol evaporates in both neutral and ionic states; $b_a^{m2} = d_a^{m2} = 0$.

Both fragmentations in the neutral state **2** and the ionic states ionized through the state **3** occur, and the state **4** $NH_4(CH_3OH)_m(NH_3)_{n-2}$ is formed through two paths such as an ammonia fragmentation from $NH_4(CH_3OH)_m(NH_3)_{n-1}$ and a methanol one from $NH_4(CH_3OH)_{m+1}(NH_3)_{n-2}$. Thus, the very complicated superposition of the time evolutions of population for the different parent clusters must be considered to explain the observed time evolutions of ion signals. By using the parameters defined above, we obtain the time evolution of $NH_4^+(CH_3OH)_m(NH_3)_{n-2}$ as follows

$$I(t;NH_4^+(CH_3OH)_m(NH_3)_{n-2}) = p_{1p}^{mn}S_1^{mn} + p_{2p}^{mn}S_2^{mn} + p_{3p}^{mn+1}b_a^{mn+1}S_3^{mn+1} + p_{3p}^{m+1n}(1 - b_a^{m+1n})S_3^{m+1n} + p_{4p}^{mn-2}[d_a^{mn+1}S_4^{mn+1} + (1 - d_a^{m+1n})S_4^{m+1n}] \quad (15)$$

while for the unprotonated ions $(CH_3OH)_m(NH_3)_n^+$

$$I(t;(CH_3OH)_m(NH_3)_n^+) = p_{1u}^{mn}S_1^{mn} + p_{2u}^{mn}S_2^{mn} p_{3u}^{mn+1}b_a^{mn+1}S_3^{mn+1} + p_{3u}^{m+1n}(1 - b_a^{m+1n})S_3^{m+1n} + p_{4u}^{mn}[d_a^{mn+1}S_4^{mn+1} + (1 - d_a^{m+1n})S_4^{m+1n}] \quad (16)$$

In fitting the experimental results to these equations, we need several parameters such as p_{ip}^{mn}, p_{iu}^{mn}, b_a^{mn}, d_a^{mn}, W^{mn}, and so on. Since fitting all the parameters by a least-squares fitting is very difficult, some assumptions are necessary. In the following section, these assumptions will be discussed.

C. Fitting Procedure and Fitting Results. In the fitting procedure, we adopt some assumptions, which should be confirmed for their validities. First, one notes that the unprotonated cluster ions are not produced by the ionization of the state **3**. Thus, it is reasonable to set p_{3u}^{mn} in eq 16 to zero, and the observed rise feature in $(NH_3)_2^+$ is attributed to the last square bracket only. According to the work by Freudenberg et al.,[27] p_{4p}^{mn} is considered to be approximately zero. They found that no contribution of state **4** to the protonated cluster signals is detected for $NH_4(NH_3)_n$. Although they have not shown the validity of this simplification, it is reasonable to consider that the excess energy in the radical pair clusters in the state **4** should be too small to eject the NH_2 unit in the ionic state after the ionization by a probe photon, because they are cooled down by the solvent evaporation.

With these assumptions, the time profiles are regarded as the superposition of three components: sharp spike, the following decay component in several picoseconds (slow-decay component), and the decay of long-lived radical (the slowly decaying tail at the longer delay time). Time constants corresponding to the above three profiles are T_1, T_2, and τ_{30}, respectively. K_2 (=1/T_2) is primarily determined by the decay curve on a time scale of 5− 20 ps, and somewhat affects a rise curve of the long-lived component. However, since the amplitude of the long-lived component is much smaller than the other two, not so much information can be obtained from the rise component in the time profile. For example, the time profile for the $NH_4^+(CH_3OH)_m(NH_3)_n$ ion has two rise components derived from the states **3** of $NH_4(CH_3OH)_{m+1}(NH_3)_n$ and $NH_4(CH_3OH)_m(NH_3)_{n+1}$, but we cannot determine the ratio of two rise components and their time constants accurately.

Since the lifetimes of radical clusters ($\tau_{30} = 1/k_{30}$) cannot be determined precisely from the time profiles on the short time scale as shown in Figure 3, we adopt the lifetimes of long-lived components obtained from the time profiles on the longer time scale in Figure 5 by assuming a superposition of a single-exponential decay and a step function. As listed in Table 1, the time profiles for $NH_4^+(CH_3OH)_m$ display the short lifetimes, while those with $n > 0$ have very long ones. Because the long-lived component in $NH_4^+(CH_3OH)_m$ is considered to be comprised of two functions derived from the states **3** of $NH_4(CH_3OH)_{m+1}$ and $NH_4(CH_3OH)_m(NH_3)_1$, the single-exponential and the step function components correspond to the population change of the state **3** of each cluster. It is concluded that the states **3** of $NH_4(CH_3OH)_m$ relax to the loss channel within a few 100 ps, and that those with $n > 0$ stay on the nanosecond or microsecond order giving the step functions to the time profiles. One notes that the long-lived component of NH_4^+ consists of the decay function of NH_4 itself as well as the superposition of the decay for $NH_4(CH_3OH)_1$ and step functions for $NH_4(NH_3)_1$. Thus, there are two candidates such as NH_4 and $NH_4(CH_3OH)_1$ responsible for the obtained lifetime of 230 ps. However, since the decomposition lifetime of NH_4 radical has been determined to be 13 ps,[26] the observed decay is attributed to that of $NH_4(CH_3OH)_1$.

Using the above fitting procedures, we obtain the time constants of T_1 (=1/K_1), T_2 (=1/K_2), and τ_{30} (=1/k_{30}) as listed in Table 2. The convoluted curves by using these time constants are shown as the solid curves in Figure 3, which agree well with the experimental pump−probe curves. Unfortunately, due to the fairly long pulse duration in the present experimental setup, the obtained T_1 includes some errors. However, a rough trend that they increase with the number of solvents is obtained. This result is consistent with the previous report about the $(NH_3)_n$ system.[27] In addition to the time profiles of $NH_4^+(CH_3OH)_m(NH_3)_n$, the above fitting procedure also successfully reproduces the data for $(NH_3)_2^+$, which is shown by a solid curve in Figure 4a. In this case, the time profile for $(NH_3)_2^+$ is composed of the sharp spike, the decay function of the state **2** of $(NH_3)_2$ with a time constant of 8.1 ps, and the rise of long-lived components from the states **4** of $(NH_3)_3$ and $(NH_3)_2(CH_3OH)_1$ with time constants of 6.5 and 14.9 ps, respectively. Similarly, as seen in Figure 4, the pump−probe data for the other unprotonated ions are also reproduced by using the parameters obtained from the above fittings. Thus, the present model is considered to be appropriate to understand the complicated dynamics for the formation and relaxation process of $NH_4(CH_3OH)_m(NH_3)_n$.

D. Relaxation Dynamics of Radical Pairs. The T_2 values in Table 2 correspond to the relaxation time constants of radical pairs formed through the $\tilde{A}$-state. From the viewpoints of the number and composition of solvents, we have realized two tendencies: the first one is the shorter T_2 with increasing number of NH_3 molecules; T_2 values of $NH_4(NH_3)_n$ are 8.1, 6.5, 4.0, and 3.5 ps for $n = 0-3$, respectively. The second is the elongation of T_2 by the solvent exchange from ammonia to methanol. Among the $(CH_3OH)_m(NH_3)_n(NH_4NH_2)^*$ clusters with the same total number of solvents ($m + n$), T_2 of the clusters containing more methanol molecules becomes longer. For example, T_2 values are 4.0, 8.3, and 9.6 ps, for $m = 0$, 1, and 2, respectively, in the case of $m + n = 2$. However, these solvation effects become much smaller for the larger clusters. In fact, the T_2 values of the larger clusters with the total solvent number of four are similar to each other. These features suggest that ammonia molecules accelerate the relaxation of radical

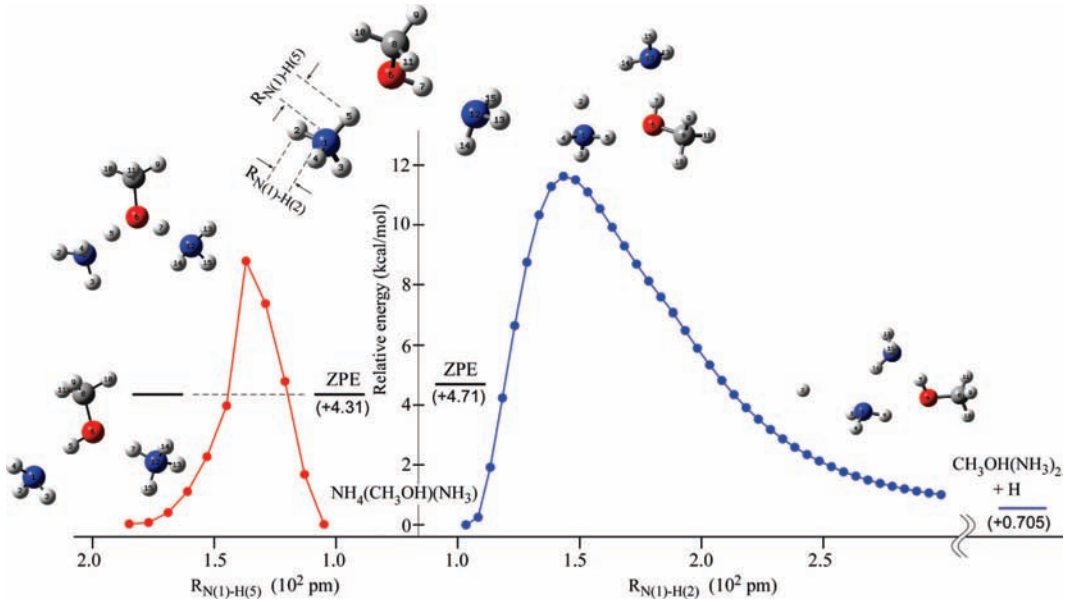

Figure 9. Calculated potential energy curves as a function of the H_3N-H distances, $R_{N(1)-H(5)}$ and $R_{N(1)-H(2)}$, in $NH_4(CH_3OH)_1(NH_3)_1$ clusters. The calculations at the MP2/6-31++G(d,p) level including basis set superposition error corrections were carried out by optimizing the cluster structures for the fixed $R_{N(1)-H(2)}$ and $R_{N(1)-H(5)}$, respectively. ZPE indicates the zero-point energy level of the reactive mode. The inserted figures of clusters are the optimized structures at characteristic steps.

pairs, while methanol solvents inhibit it. As for the origin of the solvation effect on the ejection of NH_2 and solvent evaporation, we have to consider the following two processes: (1) hydrogen-atom transfer (H-T) and (2) internal conversion.

It is suggested that the H-T within clusters may affect the ejection dynamics of the NH_2 unit from the radical pair. The generated radical-pair clusters possess the internal energy, so that the reorientation and isomerization of clusters occur. Especially, the excess hydrogen atom easily migrates through tunneling, leading to delocalization of a radical unit within the clusters. As a result of the migration of the radical site, it may increase the probability of encountering the reaction site of the NH_2 ejection. Thus, it is considered that H-T accelerates the fragmentation of NH_2. Here, the fact that the ammonia molecule is a more favorable acceptor of hydrogen atom than methanol, as mentioned in the previous section, is very important. That is to say, the hydrogen migrates within the moiety of ammonia clusters only, and H-T does not occur between ammonia and methanol. Therefore, as the relative fraction of methanol molecules in cluster increases, H-T within cluster is suppressed.

T_2 may also be affected by internal conversion. As predicted by Park and Iwata, the radical pair has no local minimum in the ground state,[19] and only the excited-state radical pair exists in the molecular beam. Thus, its relaxation to the ground-state is thought to be another loss channel, leading to shorter T_2. It is well-known that internal conversion rate in clusters become faster as the number of solvents in the cluster increases. For example, Schulz et al. reported that the lifetimes of the excited state for $Na(NH_3)_n$ are significantly shortened with increasing NH_3 molecules.[49] And the similar trend has also been observed for the lifetimes of $NH_4(NH_3)_n$.[50] Therefore, we suggest that the increase of NH_3 solvents may induce faster internal conversion, resulting in the shorter lifetime of the state **2**, i.e., T_2.

E. Relaxation Dynamics of NH_4 Radical. As seen in Table 2, the lifetimes of NH_4 radical clusters (τ_{30}) show a remarkable change by the addition of an ammonia molecule to $NH_4(CH_3OH)_m$ from about 300 ps to more than 10 ns. Concerning the lifetimes of solvated NH_4 clusters, Fuke and Takasu found that free radical has a very short lifetime of 13 ps and that the lifetimes are elongated by more than 10^6 times by the addition of NH_3 molecules.[26] They explained that this lifetime elongation is due to the suppression of the hydrogen-atom tunneling reaction, $NH_4 \rightarrow NH_3 + H$, as a result of the lager stabilization energy for NH_4 than that for NH_3. Similarly, in the CH_3OH solvation case, the lifetime of cluster is determined by the stabilization of NH_4 radical. Thus, it is concluded for the τ_{30} values of $NH_4(NH_3)_1$ and $NH_4(CH_3OH)_1$ that the solvation effect of CH_3OH to stabilize NH_4 is smaller than that of NH_3. This argument is supported by the binding energies of NH_4-NH_3 and NH_4-CH_3OH such as 3.80 and 2.83 kcal/mol, respectively, obtained by *ab initio* calculations at the MP2/6-31++G(d,p) level using the Gaussian 03 program.[51]

It is instructive to consider the difference in τ_{30} between $NH_4(CH_3OH)_1$ and $NH_4(CH_3OH)_1(NH_3)_1$. As reported in our previous paper,[41] $NH_4(CH_3OH)_1(NH_3)_1$ is likely to adopt the chain structure with terminal ammonia, $NH_4\cdots CH_3OH\cdots NH_3$. Thus, the stabilization of NH_4 radical by methanol solvent in this cluster is predicted to be similar to that in $NH_4(CH_3OH)_1$. If the rate of the tunnel reaction is determined by the degree of the stabilization of NH_4 radical only, the lifetimes of $NH_4(CH_3OH)_1$ and $NH_4(CH_3OH)_1(NH_3)_1$ would be almost the same. However, the observed τ_{30} values of these clusters are substantially different. These results may remind us of another possible origin of the lifetime elongation arising from a delocalization of hydrogen atom. For example, in $NH_4(CH_3OH)_1(NH_3)_1$, the hydrogen atom may be transferred via CH_3OH as follows: $NH_3-H\cdots CH_3OH\cdots NH_3 \leftrightarrow NH_3\cdots CH_3OH\cdots H-NH_3$, while the H-T between methanol and ammonia, $CH_3OH\cdots H-NH_3 \leftrightarrow CH_3OH_2\text{-}NH_3$, may not occur, as stated above. In Figure 9, the potential energy barrier heights of $NH_4(CH_3OH)_1(NH_3)_1$ are plotted along the reaction coordinates: $R_{N(1)-H(5)}$ and $R_{N(1)-H(2)}$. The former corresponds to the H-T between the NH_3 and the methanol within a cluster, whereas the latter corresponds to the dissociation of the hydrogen atom from the NH_4. The calculated zero-point energy levels of the NH stretching vibrations involved in the reaction coordinates are shown by bars for the stable structures. As seen in the figure,

TABLE 3: Time Constants of the Decay of $(CH_3OH)_m(NH_3)_n$* and $(CH_3OH)_m(NH_3)_{n-2}(NH_4NH_2)$* Radical Pair, T_1 (fs) and T_2 (ps), Respectively, Obtained by Least-Squares Fitting of the Time Profiles with the Probe of 395 nm

	T_1/T_2		
n	$m = 0$	$m = 1$	$m = 2$
2	210^{+80}_{-60} / 6.5 ± 0.6[a]	310^{+60}_{-70} / 5.9 ± 0.5[a]	
3	200^{+80}_{-50} / 3.3 ± 0.3[a]	270^{+70}_{-60} / 5.2 ± 0.4	
4	250^{+70}_{-60} / 3.8 ± 0.3	290^{+70}_{-70} / 5.3 ± 0.4	300^{+60}_{-60} / 5.9 ± 0.5
5	270^{+60}_{-70} / 3.9 ± 0.3	300^{+60}_{-70} / 4.9 ± 0.4	330^{+50}_{-60} / 5.6 ± 0.4
6	270^{+70}_{-70} / 4.4 ± 0.4	290^{+60}_{-70} / 4.9 ± 0.4	330^{+50}_{-70} / 4.8 ± 0.4

[a] These values have ambiguity because the time profiles include the contribution of two-photon absorption process.

the cluster containing a CH_3OH_2 form does not have a local minimum, suggesting the instability of this structure. In the longer $R_{N(1)-H(5)}$ region, the other stable structure of radical cluster is formed by the H-T to the terminal ammonia. On the other hand, the potential energy barrier along the $R_{N(1)-H(2)}$ is substantially high and also much wider compared with that along the $R_{N(1)-H(5)}$. Thus, a concerted H-T between NH_4 and the ammonia molecule located at the other side may occur through the neighboring methanol by tunneling. In the case of $NH_4(CH_3OH)_1$, the degree of freedom of hydrogen-atom migration is restricted to three hydrogen-atom elimination coordinates, $NH_3(CH_3OH) + H$, since a H-T toward methanol is suppressed. In contrast, for $NH_4(CH_3OH)_1(NH_3)_1$, another degree of freedom for hydrogen-atom migration within the cluster may open due to the relatively low energy barrier as seen in Figure 9. These arguments suggest that the anomalous elongation of the lifetime for $NH_4(CH_3OH)_1(NH_3)_1$ may be due to the hydrogen-atom migration in clusters in addition to the stabilization by solvation as mentioned in the previous paragraph.

F. Interpretation of Time Profiles for the Longer Probe Wavelength. Hertel and co-workers confirmed the validity of their kinetic model by applying it to the pump−probe data observed with the longer probe wavelength.[44] We have also examined the time profiles obtained with the probe wavelength at 395 nm using the constructed kinetic model. The probe wavelength of 263 nm (4.7 eV) can ionize all $NH_4(CH_3OH)_m(NH_3)_n$ whose IPs are 4.6−2.5 eV depending on cluster compositions,[41] while the 395 nm (3.2 eV) photon does not have enough energy to ionize the smaller clusters such as $NH_4(CH_3OH)_m(NH_3)_1$ ($m = 0-3$) and $NH_4(CH_3OH)_m(NH_3)_2$ ($m = 0-2$). In the latter cases, the obtained time profiles can be considered as the superposition of two decay components, which are the initially excited state **1** of NH_3 and the state **2** of the subsequently generated radical pairs. Thus, in the case of the smaller clusters (m, $n = 1$ or 2), the amplitude of the slowly decaying long tail is small, while those for the larger clusters are observed with appreciable intensity due to the lower IPs. Even if it is conceivable to ionize the states **3** of the relatively large clusters, the excess energy deposited in the ionic state is so small that fragmentation of solvents in the ionic state may not occur. Therefore, the observed $NH_4^+(CH_3OH)_m(NH_3)_{n-2}$ are composed of the sharp spike, slow decay function, and the rise of the long-lived component originating from the same neutral $(CH_3OH)_m(NH_3)_n$ clusters. Then, according to the kinetic model described in Figure 7, eq 15 should be modified as follows

$$I(t;NH_4^+(CH_3OH)_m(NH_3)_{n-2}) = p_{1p}^{mn}S_1^{mn} + p_{2p}^{mn}S_2^{mn} + p_{3p}^{mn}S_3^{mn} \quad (17)$$

As in the case of the fitting for the shorter-probe wavelength results, we adopt two assumptions. One of them is the negligible branching and detection probabilities p_{4p}^{mn}, as mentioned in section IV.C. The second is about the decay lifetimes of states **3** for the solvated NH_4 radical clusters, i.e., τ_{30}. Because the amplitude of the slowly decaying long tail is too small to determine τ_{30} accurately, we presuppose that the long-lived component is time independent at the longer delay time.

The solid curves shown in Figure 6 are the calculated results by using the time constants of T_1 ($=1/K_1$) and T_2 ($=1/K_2$), which are obtained by least-squares fittings. The obtained time constants are listed in Table 3. The results indicate that the dependence of the lifetimes on the number and composition of solvents for the 395 nm probe are smaller than those for the shorter probe wavelength case. Especially, the tendency that T_2 values are elongated with the addition of ammonia molecules is hardly observed at all. Moreover, for the smaller clusters, the lifetime difference between two probe wavelengths is remarkable; the lifetimes probed at 395 nm are much shorter. Hertel and co-workers have found that the lifetimes of radical-pair clusters solvated with ammonia molecules, $(NH_3)_n(NH_4NH_2)$*, are shortened from 4 to 2 ps, by changing the probe wavelength from 266 to 400 nm.[27,44]

It is not easy to explain the dependence of lifetimes on the probe wavelength. One of the possible explanations may be that the experiments with two probe wavelengths monitor different dynamics with different internal energies. Because the IP of the solvated radical pair may be smaller than 395 nm (3.2 eV), Franck−Condon transition with the 263-nm photon is able to ionize the state with smaller internal energy, compared to 395 nm. The state with smaller internal energy is difficult to induce further reactions such as the NH_2 ejection and solvent evaporation, because of the difficulty in overcoming the energy barrier for dissociation. Therefore, it is suggested that T_2 measured by the probe wavelength at 263 nm may provide longer lifetimes. From these results, it is considered that the dynamics with similar internal energy is monitored for larger clusters, since the energy gap between neutral and ionic state becomes smaller. Consequently, the dependence of lifetimes on the probe wavelengths is expected to become smaller as the cluster size increases. This prediction is in accord with the trend for the observed lifetimes. These arguments indicate the validity of the present kinetic model even for the methanol−ammonia mixed clusters.

V. Conclusions

The real-time observations of the ultrafast reaction dynamics after the excitation to the Ã-state of the neutral $(CH_3OH)_m(NH_3)_n$ mixed clusters have been carried out by means of femtosecond time-resolved pump−probe spectroscopy. It is found that the dynamics after the photolysis of $(CH_3OH)_m(NH_3)_n$ progresses in the sequential three step. The first step is the ultrafast hydrogen-atom transfer (H-T) between NH_3-NH_3 in the excited Ã-state, resulting in the radical pair (NH_4NH_2)*, the second is the relaxation process of radical-pair clusters including the ejection of NH_2 unit, the solvent evaporation, and the internal conversion. The last step is the hydrogen-atom elimination from the solvated NH_4 clusters produced after the above NH_2 ejection. The fact that the unprotonated $(CH_3OH)(NH_3)^+$ ion exhibits no rise component in contrast to the ammonia dimer ion clearly indicates that the H-T between ammonia and methanol is

suppressed, meaning the unfavorable formation of radical pair, (CH_3OH_2−NH_2).

The remarkable dependence of lifetimes on the number and composition of solvents is found in the second and third steps. The reaction rate constants in the second step become smaller with increasing number of NH_3 solvents. On the other hand, the solvent exchange of ammonia to methanol provides longer lifetimes. These features are explained by the following two reasons: H-T within clusters and internal conversion. The third relaxation step is attributed to the hydrogen-atom elimination from the NH_4 radical, which is inhibited by the solvation of single ammonia. It is suggested that the ammonia solvent induces a larger stabilization effect to NH_4 radical than methanol and that the delocalization of a hydrogen atom within the $NH_4(NH_3)_n$ moiety leads to the slower hydrogen-atom elimination in contrast to no hydrogen delocalization into methanol moiety due to unstable CH_3OH_2 radical.

The dependence of the time profiles on the probe wavelength stems from the different ionization efficiency, which depends on monitoring the different states of the solvated radical clusters possessing different internal energy. In spite of the largely different energy of the probe photons, the experimental results can be explained by using the constructed kinetic model. Thus, the constructed model describes the generation and relaxation dynamics of the NH_4 radical clusters very well.

Acknowledgment. This work is partially supported by the Grant-in-Aid for Scientific Research (grant no. 18350009) and by the Grant-in-Aid for Scientific Research in Priority Areas (grant no. 19056004) from the Ministry of Education, Culture, Sports, Science, and Technology (MEXT) of Japan, and also a research grant for the Japan Science and Technology Agency. Y.Y. is supported by the postdoctoral research fellowship of the Japan Society for the Promotion of Science (grant no. 19000475).

References and Notes

(1) Odutola, J. A.; Dyke, T. R.; Howard, B. J.; Muenter, J. S. *J. Chem. Phys.* **1979**, *70*, 4884.
(2) Stephan, K.; Futrell, J. H.; Peterson, K. I.; Castleman, A. W., Jr.; Wagner, H. E.; Djuric, N.; Mark, T. D. *Int. J. Mass Spectrom. Ion Phys.* **1982**, *44*, 167.
(3) Buck, U.; Lauenstein, Ch. *J. Chem. Phys.* **1990**, *92*, 4250.
(4) Ceyer, S. T.; Tiedemann, P. W.; Mahan, B. H.; Lee, Y. T. *J. Chem. Phys.* **1979**, *70*, 14.
(5) Shinohara, H.; Nishi, N.; Washida, N. *J. Chem. Phys.* **1985**, *83*, 1939.
(6) Kaiser, E.; de Vries, J.; Steger, H.; Menzel, C.; Kamke, W.; Hertel, I. V. *Z. Phys. D* **1991**, *20*, 193.
(7) Echt, O.; Dao, P. D.; Morgan, S.; Castleman, A. W., Jr. *J. Chem. Phys.* **1985**, *82*, 4076.
(8) Misaizu, F.; Houston, P. L.; Nishi, N.; Shinohara, H.; Kondow, T.; Kinoshita, M. *J. Phys. Chem.* **1989**, *93*, 7041.
(9) Kamke, W.; Herrmann, R.; Wang, Z.; Hertel, I. V. *Z. Phys. D* **1988**, *10*, 491.
(10) Ceyer, S. T.; Crofton, P. W.; Lee, Y. T. *J. Phys. Chem.* **1991**, *95*, 2182.
(11) Misaizu, F.; Houston, P. L.; Nishi, N.; Shinohara, H.; Kondow, T.; Kinoshita, M. *J. Chem. Phys.* **1993**, *98*, 336.
(12) Farmanara, P.; Radloff, W.; Stert, V.; Ritze, H.-H.; Hertel, I. V. *J. Chem. Phys.* **1999**, *111*, 633.
(13) Radloff, W.; Hertel, I. V. *Rep. Prog. Phys.* **2006**, *69*, 1897.
(14) Wei, S.; Purnell, J.; Buzaza, S. A.; Stanley, R. J.; Castleman, A. W., Jr. *J. Chem. Phys.* **1992**, *97*, 9480.
(15) Zhong, Q.; Castleman, A. W., Jr. *Chem. Rev.* **2000**, *100*, 4039.
(16) Hirao, K.; Fujikawa, T.; Konishi, H.; Yamabe, S. *Chem. Phys. Lett.* **1984**, *104*, 184.
(17) Tomoda, S. *Chem. Phys.* **1986**, *110*, 431.
(18) Cao, H. Z.; Evleth, E. M.; Kassab, E. *J. Chem. Phys.* **1984**, *81*, 1512.
(19) Park, J. K.; Iwata, S. *J. Phys. Chem. A* **1997**, *101*, 3613.
(20) Greer, J. C.; Ahlrichs, R.; Hertel, I. V. *Z. Phys. D* **1991**, *18*, 413.
(21) Amor, N. B.; Maynau, D.; Spiegelmann, F. *J. Chem. Phys.* **1996**, *104*, 4049.
(22) Ziegler, L. D. *J. Chem. Phys.* **1985**, *82*, 664.
(23) Fuke, K.; Yamada, H.; Yoshida, Y.; Kaya, K. *J. Chem. Phys.* **1988**, *99*, 5238.
(24) Wei, S.; Purnell, J.; Buzaza, S. A.; Castleman, A. W., Jr. *J. Chem. Phys.* **1993**, *99*, 755.
(25) Purnell, J.; Wei, S.; Buzaza, S. A.; Castleman, A. W., Jr. *J. Phys. Chem.* **1993**, *97*, 12530.
(26) Fuke, K.; Takasu, R. *Bull. Chem. Soc. Jpn.* **1995**, *68*, 3309.
(27) Freudenberg, Th.; Radloff, W.; Ritze, H.-H.; Stert, V.; Weyers, K.; Noack, F.; Hertel, I. V. *Z. Phys. D* **1996**, *36*, 349.
(28) Herzberg, G. *Faraday Discuss. Chem. Soc.* **1981**, *71*, 165.
(29) Herzberg, G. *J. Astrophys. Astron.* **1984**, *5*, 131.
(30) Whittaker, E. A.; Sullivan, B. H.; Bjorklund, G. C.; Wendt, H. R.; Hunziker, H. E. *J. Chem. Phys.* **1984**, *80*, 961.
(31) Hertel, I. V.; Hüglin, C.; Nitsch, C.; Schulz, C. P. *Phys. Rev. Lett.* **1991**, *67*, 1767.
(32) Takasu, R.; Misaizu, F.; Hashimoto, K.; Fuke, K. *J. Phys. Chem. A* **1997**, *101*, 3078.
(33) Salter, T. E.; Mikhailov, V.; Ellis, A. M. *J. Phys. Chem. A* **2007**, *111*, 8344.
(34) Dauster, I.; Suhm, M. A.; Buck, U.; Zeuch, T. *Phys. Chem. Chem. Phys.* **2008**, *10*, 83.
(35) Fuke, K.; Takasu, R.; Misaizu, F. *Chem. Phys. Lett.* **1994**, *229*, 597.
(36) Nonose, S.; Taguchi, T.; Mizuma, K.; Fuke, K. *Eur. Phys. J. D* **1999**, *9*, 309.
(37) Nonose, S.; Taguchi, T.; Chen, F.; Iwata, S.; Fuke, K. *J. Phys. Chem. A* **2002**, *106*, 5242.
(38) Kassab, E.; Evleth, E. M. *J. Am. Chem. Soc.* **1987**, *109*, 1653.
(39) Kassab, E.; Evleth, E. M. *Pure Appl. Chem.* **1988**, *60*, 209.
(40) Daigoku, K.; Miura, N.; Hashimoto, K. *Chem. Phys. Lett.* **2001**, *346*, 81.
(41) Yamada, Y.; Nishino, Y.; Fujihara, A.; Ishikawa, H.; Fuke, K. *Chem. Phys. Lett.* **2008**, *459*, 65.
(42) Sominska, E.; Gedanken, A. *J. Mol. Spectrosc.* **1996**, *175*, 234.
(43) Bobbert, C.; Schütte, S.; Steinbach, C.; Buck, U. *Eur. Phys. J. D* **2002**, *19*, 183.
(44) Freudenberg, Th.; Radloff, W.; Ritze, H.-H.; Stert, V.; Noack, F.; Hertel, I. V. *Z. Phys. D* **1997**, *41*, 267.
(45) Williams, B. W.; Porter, R. F. *J. Chem. Phys.* **1980**, *73*, 5598.
(46) Gellene, G. I.; Porter, R. F. *J. Chem. Phys.* **1984**, *88*, 6680.
(47) Jeon, S.-J.; Raksit, A. B.; Gellene, G. I.; Porter, R. F. *J. Am. Chem. Soc.* **1985**, *107*, 4129.
(48) Chen, F.; Davidson, E. R. *J. Phys. Chem. A* **2001**, *105*, 10915.
(49) Schulz, C. P.; Höhndorf, J.; Brockhaus, P.; Noack, F.; Hertel, I. V. *Chem. Phys. Lett.* **1995**, *239*, 18.
(50) Okai, N.; Takahata, A.; Morita, M.; Nonose, S.; Fuke, K. *J. Phys. Chem. A* **2004**, *108*, 727.
(51) Frisch, M. J.; Trucks, G. W.; Schlegel, H. B.; et al. *Gaussian 03*, Revision E.01; Gaussian, Inc.: Wallingford, CT, 2004.

JP810266A